Journal of Power Sources 270 (2014) 349–358

Contents lists available at ScienceDirect

Journal of Power Sources

journal homepage: www.elsevier.com/locate/jpowsour

Experimental performances of a battery thermal management system using a phase change material

Charles-Victor Hémery [a, b, *], Franck Pra [a], Jean-François Robin [a], Philippe Marty [a, b]

[a] CEA, LITEN/DTS/LETh, 17, rue des Martyrs, 38054 Grenoble Cedex, France
[b] UJF-Grenoble 1/Grenoble-INP/CNRS, LEGI UMR 5519, Grenoble F-38041, France

HIGHLIGHTS

- The PCM integration is new and the PCM quantity is minimized.
- The cell casings are used in order to evacuate/bring the heat inside the cell.
- Heat exchange is improved because of the coupling with a liquid cooling system.
- Quick PCM solidification is performed during a 2C fast charge and the safety is enhanced.
- The system is fully passive and supports a complete discharge of the battery.

ARTICLE INFO

Article history:
Received 15 April 2014
Received in revised form
11 June 2014
Accepted 22 July 2014
Available online 30 July 2014

Keywords:
Li-ion batteries
Thermal management
Phase change material
Semi-passive cooling
Failure conditions
Liquid-cooling

ABSTRACT

Li-ion batteries are leading candidates for mobility because electric vehicles (EV) are an environmentally friendly mean of transport. With age, Li-ion cells show a more resistive behavior leading to extra heat generation. Another kind of problem called thermal runway arises when the cell is too hot, what happens in case of overcharge or short circuit. In order to evaluate the effect of these defects at the whole battery scale, an air-cooled battery module was built and tested, using electrical heaters instead of real cells for safety reasons. A battery thermal management system based on a phase change material is developed in that study. This passive system is coupled with an active liquid cooling system in order to initialize the battery temperature at the melting of the PCM. This initialization, or PCM solidification, can be performed during a charge for example, in other words when the energy from the network is available.

1. Introduction

Li-ion batteries are leading candidates for mobility because electric vehicles (EV) are an environmentally friendly means of transport. During battery operation, each cell warms up because of ohmic and chemical reaction heating as main heat sources [1]. A Li-ion battery has a quite limited energy density in comparison to a fuel tank for an internal combustion engine. Consequently, the battery size must be minimized, which possibly creates a thermal imbalance from one cell to another. According to the electrochemical behavior of the cells, thermal imbalance leads to heterogeneities of aging [2] and state of charge [3]. Therefore, battery thermal management systems (BTMS) are needed to control the temperature field of all the cells, enhancing safety and lifespan, and even reducing its size [4].

Nowadays, most of the EVs have air-cooling BTMS, but this kind of technology shows some drawbacks as the fan power, which depletes battery energy, and induces a large thermal imbalance between the downstream cells, which are always hotter than the upstream ones. Many others BTMS, as liquid cooling, heat pipes, thermoelectric modules, or phase change material (PCM) are listed in literature [5]. Each of them presents disadvantages such as difficult sustainment, expensive integration or limited effectiveness in terms of thermal uniformity [6]. Phase change materials seem to be a suitable solution because of the quite constant temperature of the phase transition. They can fulfill the different objectives of the BTMS, which are (1) maintaining the battery cell temperatures below the allowed maximum temperature, often 60 °C, and over a too cold temperature, −20 °C, limiting battery performances

* Corresponding author. CEA, LITEN/DTS/LETh, 17, rue des Martyrs, 38054 Grenoble Cedex, France. Tel.: +33 (0)4 38 78 32 86; fax: +33 (0)4 38 78 51 61.
E-mail address: cvhemery@hotmail.fr (C.-V. Hémery).

http://dx.doi.org/10.1016/j.jpowsour.2014.07.147
0378-7753/

[7–10], (2) minimization of the temperature difference between cells, (3) and the temperature sustainment of cells within the best operating range (25–30 °C) [11,8]. The improvement of performance and lifespan of the battery can be further improved by the choice of the operation temperature. For instance, the SEI decomposition can begin at 69 °C, according to the electrolyte composition [12]. Battery aging is intensified for a temperature over 45 °C [13]. So Sievers et al. [14] explain that the optimum operating temperature range is between 25 °C and 30 °C, and the cell temperature difference do not exceed 10 °C.

Kizilel et al. [15,16] and Sabbah et al. [17], have compared air-cooling and a battery thermal management with PCM, respectively with numerical and experimental approaches. Their PCM battery thermal management system differs from the one described here. First, the PCM filled completely the battery module. Then the PCM thermal conductivity is enhanced by a graphite matrix. Finally, the melting temperature range is widely higher because it is about 42–45 °C in Refs. [15,16], and 52–55 °C in Refs. [16,17], so the application is quite different. These melting temperature ranges interrupt the cell temperature rise before the limit recommended by battery manufacturers. But they do not show a great interest for lower temperature, where batteries are more often used, because the discharge capacity is reduced compared to air cooling. Moreover, it is important to know the thermal behavior of a battery during discharge driving cycles, which have a lower thermal impact than galvanostatic fast charge (at 2C rate for example). Because of the use of electric heaters replacing real cells, the cell discharge capacity difference between air cooling system and PCM thermal management cannot be estimated here. Kizilel et al. [15] show a reduction of 24% of the capacity fading with PCM for 300 cycles. Although their system has some shortcomings, they opened the way for efficient thermal management system. Furthermore, it seems difficult for a fully passive system with PCM to reach all the battery thermal management criteria, while some high electric appeals can occur, as a fast charge following a driving cycle discharge, which has already melted the PCM. That is why the PCM system presented here is coupled with liquid cooling plates. So it is possible to solidify PCM while the car is charging (without impact for the state of charge), or to slow down increase or decrease of temperature under external hot or cold conditions while the car is parked. Nelson et al. [9] conclude that a thermal management system is necessary at all times during the life of the battery, the vehicle being moving or not, whether it is summer or winter. So if the heat power cannot be evacuated from the module or provided to the cells for cold cranking, PCM becomes a drawback because of its large thermal inertia.

Two experimental tests sections were built to simulate the thermal behavior of a 27 cells module of type 26650 with an air cooling, and with a new PCM integration. Electrical heaters introduced in cylindrical holders replace real cells. The experimental setup can simulate constant charge or discharge, some short driving cycles, and thermal defects, as, low power thermal failure, of the cell at the center of the module. The wall temperature of each cell is measured. The study presented here is a comparison between the behavior of an air-cooled battery module under usual or thermal failure conditions, and one another with PCM. Compared to Al-Hallaj co-writers technology [15–19], which showed good performances, the main benefit of the PCM's prototype presented here is the use of liquid cooling in order to control the module temperature. It can be used when the car is charging, and so the module is operated at the melting temperature of the PCM during driving. The temperature of all cells in the module is equal. Comparatively to an air cooling system, the PCM's prototype has shown really promising behavior under failure tests.

2. Experimental setup

The description of the experimental setup is divided into three parts. Common parts of the test benches as regulators, power supplies, thermo-regulated bath, electric heaters in casing, and data acquisition allows producing comparable results between the both tests sections are described in the first part. The second part concerns the air cooling test section, and the third part relates to the semi-passive tests section.

2.1. Description of the common parts

For safety reasons, the cells used in the module are not real ones. Electric heaters embedded in stainless steel cases replace Li-ion cells. The size of the casing is identical to real 26650 Li-ion cells. A temperature sensor (platinum probe, ± 0.06 °C at 0 °C) is placed on the wall of each casing to get individual thermal response. Twenty-seven heaters are used in both tests sections. It is the minimum setup in order to estimate the interactions between cells in a longitudinal air cooling configuration.

Twenty-six heaters of the module are connected in series to a power supply (300 V–2.8 A). Another identical power supply is devoted to the last cell, located at the center of the module. It allows simulating thermal defects, higher thermal power, up to simulation of low power thermal failure. Two programmers govern the power supplies. They provide constant current requests or simulations of driving cycles. High power defects, as thermal runaway on a real cell, cannot be tested with the bench for compactness reasons, in order to simulate a real battery module size.

All the data are recorded by two Agilent 34970A data loggers connected to a computer.

2.2. Air cooling test section

A simplified scheme of the air cooling experimental setup is presented in Fig. 1:

An air compressor produces the air flow. A regulated flowmeter measures the flow rate from 0 to 30 N m^3 h^{-1} (30 ± 0.27 N m^3 h^{-1}). A second flowmeter, coupled with a control valve estimates the flow rates included between 30 and 100 N m^3 h^{-1} (100 ± 1.7 N m^3 h^{-1}). A thermo-regulated bath with circulator, combined to a heat exchanger, controls air inlet temperature.

A honeycomb filter located at the inlet of the test section produces a uniform flow before the battery module inlet. The inlet and outlet diffusers include an angle (2θ) of 15° to ensure flow steadiness and low pressure drop [20]. The pressure ($1.6 \pm 8.00.10^{-3}$ bar) is recorded in addition to the battery module pressure drop (300 ± 0.225 mbar). Air temperature is measured at the inlet, the outlet and inside the module around the center cell. Since the temperature differences are supposed to be quite limited, platinum temperature probes are used (±0.06 °C at 0 °C). The cells rest on drilled aluminum plates, in order to keep a 1 mm distance between cells perpendicularly to the flow. In the longitudinal direction, there is 5 mm distance between cells because of the intrusion of the air temperature probes. The module is a combination of 27 cells spread on a cube with 3 cells edge (see Fig. 1). In order to improve the heat exchange between the air flow and the battery module, the air flows longitudinally through the cells.

The air temperature is measured by four platinum probes (±0.06 °C at 0 °C), at the inlet, the outlet of the battery module, and inside, around the center cell (1 mm distance).

2.3. Semi-passive test section

Commercial paraffin wax (Rubitherm RT28 HC) has been chosen as a phase change material. It shows many benefits as no safety

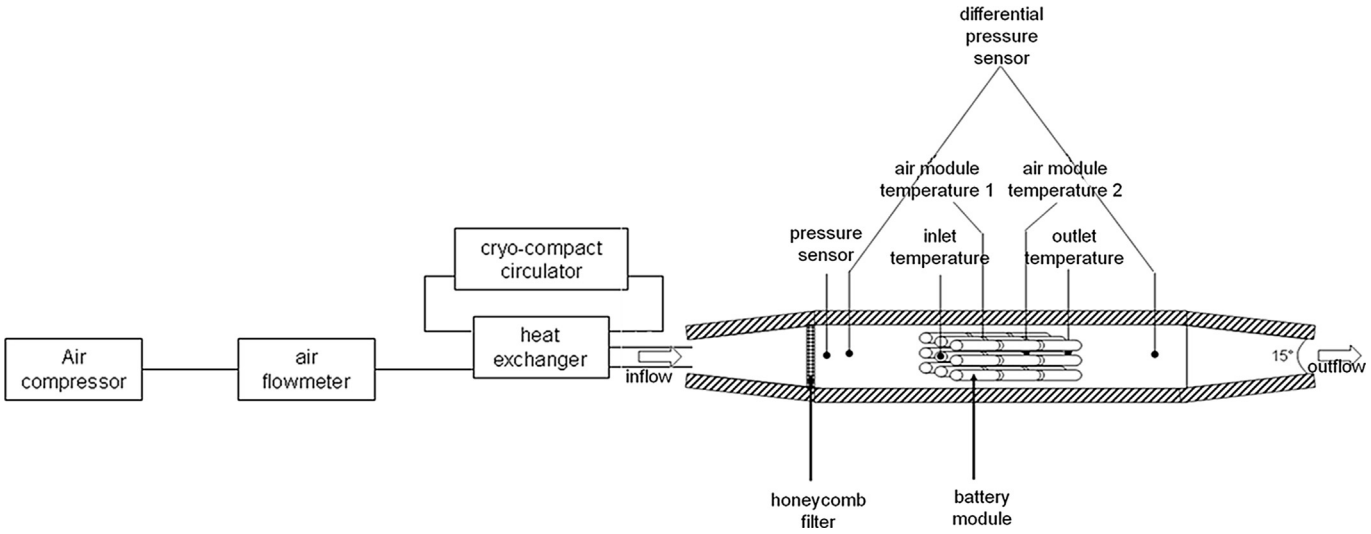

Fig. 1. Scheme of the air cooling experimental apparatus.

concerns within a large temperature range, and it is non-corrosive [21]. The phase transition temperature of that paraffin wax is 28 °C, what is suitable within the temperature range recommended by Ref. [14] for a good thermal management of the battery. The choice of that melting temperature should optimize the performance of the battery by enhancing the electrochemical reaction in cold environment. It includes a wide safety temperature range up to the battery manufacturers safety limit of 60 °C. The second thermal benefit of that PCM is its large latent heat of 245 kJ kg^{-1}. So a large part of heat can be stored in a quite low volume and light weight. In order to keep a cell at a constant temperature under a 3C discharge rate, lower than 2 mm PCM thickness is adequate. No need to fill the whole space between cylindrical cells, because the PCM is not use, and adds weight. Aluminum cans were developed to keep the good quantity of PCM and to extract heat from the battery module. At this time, the cans are still too heavy, but a weight reduction by half or more is assumed to be feasible.

All the cells are enclosed into aluminum cans in the semi-passive test section (Fig. 2).

The cans are fitted with heat transfer fins (2 mm depth) in order to bring, or to evacuate heat in the PCM. During the filling stage, the PCM is introduced into liquid phase between the electric heater casing and the can. The top and the bottom of the can are sealed with lids allowing the wires passage (or tabs in case of real cells). The 27 cells are setup in staggered rows in the test section, without gap distance, in the purpose of a maximum compactness (Fig. 3). Two cooling copper plates circulated with water in are respectively setup below and over the cans.

The plates could be made of aluminum to decrease the mass of the thermal management system. A good thermal contact is held by the lids between the cans and the plates. Water has been chosen for the liquid cooling, because it is widely used for such applications. A counter water flow pattern is applied in order to enhance balance of temperature between the cells. The water temperature is controlled by the thermo-regulated bath with circulator, and measured at the inlet and the outlet of the test section with two platinum probes (±0.06 °C at 0 °C). A flowmeter (9–150 L min^{-1} ± 1.5 L min^{-1}) measures the flow of water.

2.4. Preliminary tests

The heat power of the electric heaters must be estimated before measurements, in the purpose to be representative of real 26650 $LiFePO_4$/C cells. So, temperatures were measured on the wall of a $LiFePO_4$/C cell, and inside on the cylinder axis. Because of the intrusive measurement of the core temperature, internal thermal resistance was increased, owing to electrolyte depletion [22], if the thermocouple is not sheathed [23]. Fig. 4 shows the comparison of temperature measured on a real cell, and temperature estimated on the electrical heater wall.

The heat power was estimated based on a final temperature which was measured between the core temperature and the wall temperature of the real cell. At a 0.5C rate, two values (0.12 and 0.16 W) of the heat power gave respectively a final temperature higher than the core, or colder than wall temperature of the real cell, which respectively correspond to case number 1 and number 2 in Fig. 4. The mean value of the heat power was chosen to simulate the thermal response. So, at 0.5C the heat power value used during the simulations was 0.14 W, 0.30 W for 1C, 1.30 W for 2C and 2.75 W for 3C. At low C-rates, the curves of heater wall temperature do not match those on a real cell, because the experimental setup cannot

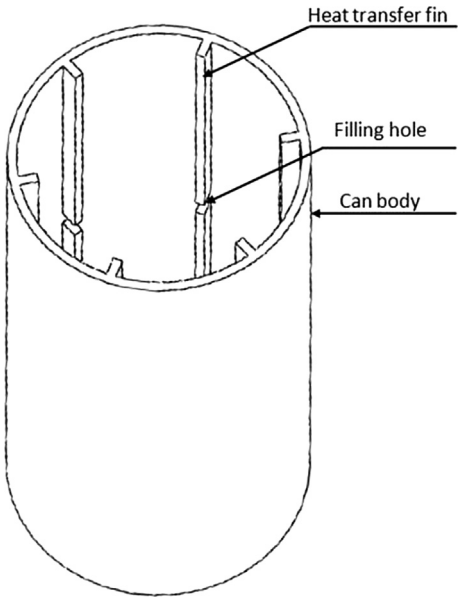

Fig. 2. Body of a can containing PCM.

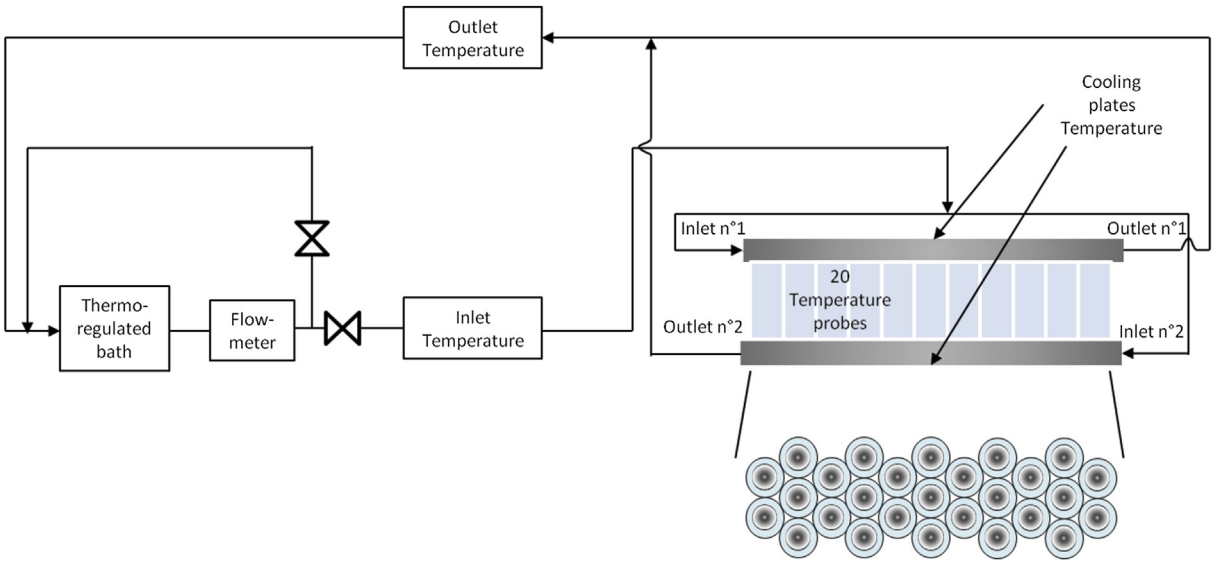

Fig. 3. Experimental setup of the semi-passive BTMS.

simulate temperature fluctuations induced by heat of reaction. These power values were used to describe a driving cycle with large power demand, corresponding to high difference in altitude.

2.5. Description of the driving cycle

All the tests were run using the same driving cycle repeated five times. Two kinds of tests were performed. A usual condition test was run with the same power in all cells in the module. A second test was performed with thermal failure occurring after 10 min of driving cycle, with a constant power value of 11.1 W (8.5 times over the maximum power of the other cells), in the cell at the center of the module. The mean electric power generated under test of usual condition and thermal failure test are shown in Fig. 5.

In a real case, state of charge of the battery allowed less than three complete driving cycles (After 2.7 cycles, SOC = 7%). During thermal failure of the cell at the center, the other cells of the module follow their succession of driving cycles.

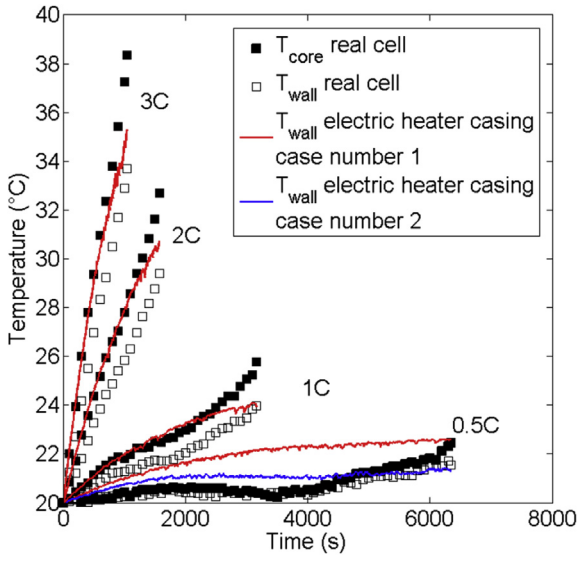

Fig. 4. Heat power estimation for simulation tests depending on C-rate.

3. Results and discussion

The results are presented in different parts. The first part describes the comparison between the temperature uniformity with and without PCM. It begins with air flow characterization before the comparison of temperature uniformity between the two systems during usual and failure conditions. The last two parts concern the fan power requirement and the performance of PCM solidification.

3.1. Comparison of temperature uniformity

Before comparing the two battery thermal management systems, the air flow is characterized for the three inlet velocities chosen, in order to be representative of literature data and a real battery pack.

The air flow rate value is modified in a reasonable range of speed used in automotive industry. The flow rates and the air velocities are presented in Table 1:

Table 1 shows the different values of the inlet velocities used for cooling the battery module. It presents Reynolds Number (the Prandtl Number for air is 0.7) estimated with variable air physical properties. To calculate the Nusselt Number, the longitudinal interstice between cells is supposed to be a pipe, and heat transfer coefficients were deduced. For laminar flow with a velocity inlet of 1 m s^{-1}, the correlation of Sieder and Tate has been used to estimate the Nusselt Number. For turbulent flow, the Colburn correlation has been used.

The heat transfer coefficient for an inlet velocity of 1 m s^{-1} can be compared to the value of 20 W m^{-2} K^{-1} used by Katheeb et al. [19] for a battery module for an electric scooter. For an inlet velocity of 2 m s^{-1}, in other words, a module internal velocity of 7.9 m s^{-1}, the heat transfer coefficient value is 55 W m^{-2} K^{-1} is similar to that one estimated by Kim and Pesaran [24] for an internal velocity of 6.3 m s^{-1}.

3.1.1. Usual conditions

As it was described previously, two tests were done on the battery module. The first one, which is discussed here, concerns the usual conditions. The second test will be presented in the next part and relates to failure condition.

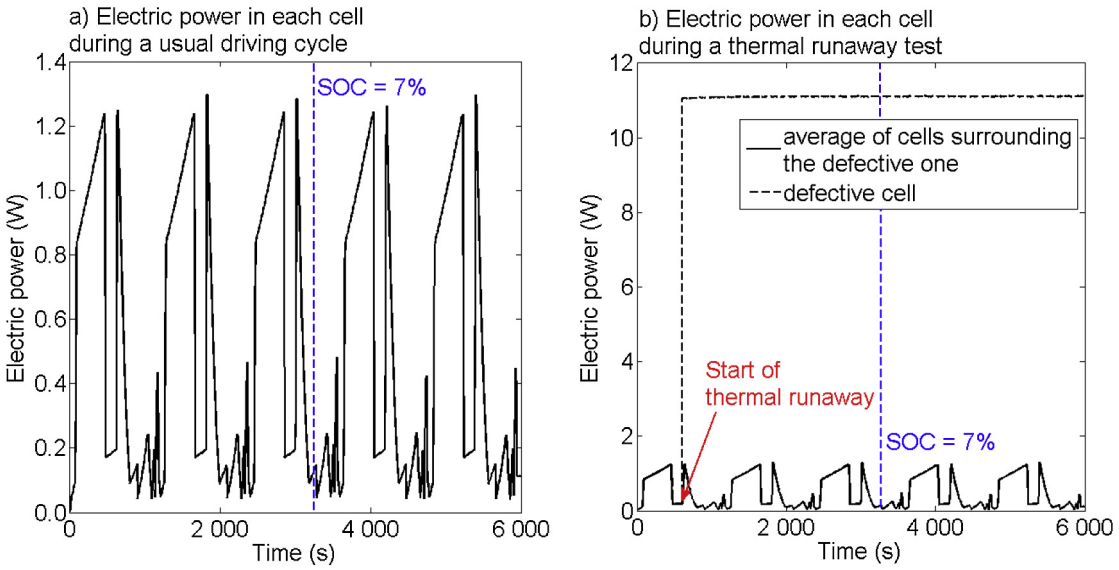

Fig. 5. Electric power in each cell during both types of cycle.

The levels of the temperature with different flow rates and PCM management systems are compared in Fig. 6.

The thermal response of the five consecutive driving cycles appears clearly in Fig. 6 for the five different curves. Each cycle can be distinguished by a large peak among which two small peaks are visible at the summit. Under natural convection, the average temperature increases constantly from the beginning of the test until the end of the fifth cycle. After 2.7 driving cycles, average temperature of all cells in the module is 35.5 °C, therefore average temperature has increased of 8.5 °C. Under natural convection, the hottest point in the module should be located on the cell at the center in that cubic geometry. In fact, the upstream cell is slightly hotter. A small residual flow between the inlet and the outlet is suspected. The more the flow rate is increased, the more the temperature decreases. So with 2 or 3 m s^{-1} inlet velocity, average module temperature is quite similar for the five cycles. From 2 m s^{-1}, convection resistance becomes small compared to the conductive resistance to the inside of the battery. It means that thermal conduction limits the heat exchange and that is useless to increase the air velocity.

The initial temperature is 27 °C. So, before melting at 28 °C, the PCM temperature has increased of 1 °C. Then four cycles are performed at constant temperature between 28 and 29 °C. At the end of the fourth cycle, the PCM is completely melted because the temperature increases at the fifth cycle to about 2 °C. The level of temperature with PCM is strictly the same than the one with a 3 m s^{-1} forced convection, with lower temperature fluctuations. So the PCM battery thermal management system shows interesting performances under driving usual conditions.

Fig. 7 shows the maximum temperature difference between the hotter and the colder cell, which is representative of the uniformity of the temperature field in the battery module. Two values of the temperature difference are shown. The first one is the maximum temperature difference while the electric car is driven. The second value represents the maximum temperature difference over five cycles. So it is possible to see the effect of a PCM fully melted over the temperature uniformity in the battery module. In that case, the liquid PCM enlarges the discrepancy of the temperature in the battery module.

The temperature difference during the driving time, and over five cycles is significantly improved with the flow rate. So the temperature difference is divided by five when the inlet velocity is multiplied by three. An air inlet velocity of 3 m s^{-1} has not a noticeable impact on module temperature uniformity compared to 2 m s^{-1}. Over the same time range, the PCM battery management system produces the best temperature uniformity within the module with a temperature difference of 0.5 °C. When the PCM is fully melted, the temperature uniformity is similar to the result estimated with an inlet velocity of 2 m s^{-1}. At first, the temperature discrepancy obtained with air cooling system seems to be adequate in terms of battery thermal management system, but the tests bench proposed here represents a small battery module. Using the same cells as the one used in this study, CEA has powered a car with 2000 cells what is much greater than the 27 cells module tested here. So, between the upstream cells and the downstream ones, the temperature difference should be widely enlarged in the entire battery pack. A particular case will be presented in Part 3.2.

One of the strong points of this study is the number of temperature probes. The PCM management system shows a small temperature difference between cells, but it is interesting to know if there is a geometric effect or not, with a hot point at the center of the module as it should be in case of natural convection.

Table 1
Air flow properties.

Inlet air velocity (theoretical value) (m s^{-1})	Air flow rate (m^3 h^{-1})	Inlet air velocity (measured) (m s^{-1})	Inlet air velocity (estimated from flow rate) (m s^{-1})	Module internal air velocity (m s^{-1})	Reynolds number	Nusselt number	Heat transfer coefficient (W m^{-2} K^{-1})
0.0	0.0	0.0	0.0	0.0			
1.0	19.4 ± 0.4	0.9 ± 0.1	0.8	3.0 ± 0.1	1140.0 ± 40.0	5.3 ± 7.1 10^{-2}	23.0 ± 6.4 10^{-1}
2.0	51.3 ± 2.7	1.9 ± 0.1	2.1	7.9 ± 0.5	2980.0 ± 140.0	12.3 ± 4.5 10^{-1}	55.0 ± 2.0
3.0	80.4 ± 5.0	2.8 ± 0.1	3.3	12.4 ± 0.9	4680.0 ± 240.0	17.6 ± 7.2 10^{-1}	78.0 ± 4.0

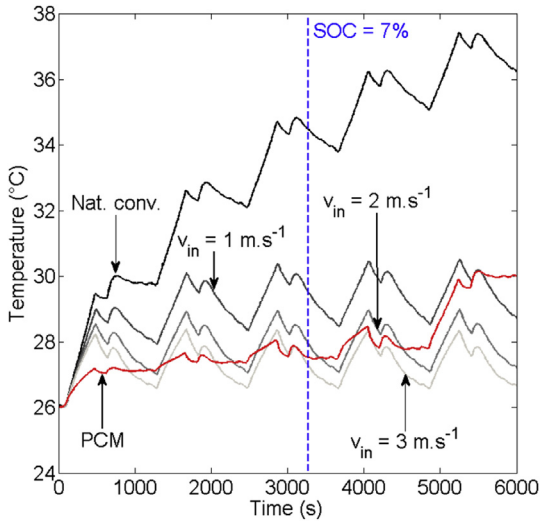

Fig. 6. Comparison of average cells module temperature with different thermal management systems.

Fig. 8 shows the temperature evolution in the entire battery module during driving cycle. Natural convection generates a large temperature unbalance between cells, with a hot point at the center of the module. Forced convection moves the hot point at the downstream of the module for the 3 theoretical air inlet velocity values. In the case of passive thermal management system, a temperature difference appears in the battery module at 4685 s, but the battery is not working anymore as there is no more energy embedded. That happened a few seconds before the last driving cycle and so the PCM should be widely melted. So the heat storage process changes. The heat is no more stored in a latent form, but in a sensible way, which is widely worst in terms of heat storage. This explains why low temperature heterogeneities arise between cells. In Fig. 8e, white cells denote sensors broken.

3.1.2. Failure conditions

The concept of thermal failure describes a phenomenon similar to a thermal runaway of a real Li-ion cell, but of lower intensity in this article. Two reasons are responsible for this behavior. The first one is the need of compactness in order to be representative of a real battery module. The second one is the fragility of some electric connections in the experimental setup, which melted under higher power values. Fig. 9 shows a comparison of the temperature rise under natural convection and results obtained with modeling or experimental tests from different authors from literature data.

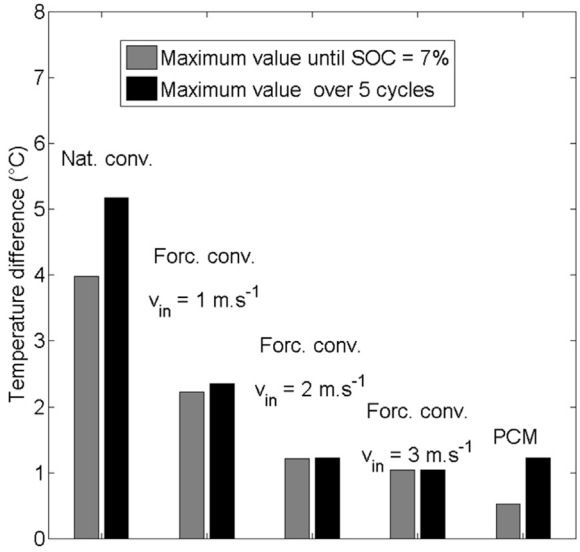

Fig. 7. Maximum temperature difference depending on the battery thermal management system.

Leising et al. [25] studied the wall temperature of a 1.5 Ah $LiCoO_2$/C prismatic cell during a short circuit caused by a low electric resistance connecting the battery terminals. The wall temperature rises up to 93.9 °C in 3 min and 30 s (Fig. 9a), which is really more intensive and faster than the wall temperature rise during the test described here. The Li-ion cell used by Leising et al. [25] shows smaller capacity than the 2.3 Ah cell simulated here, so the thickness of the cell is smaller too (13 mm, compared to a 26 mm diameter for the electric heater in casing). That thickness difference, associated to the very low equivalent thermal conductivity in the perpendicular direction of the electrodes and to the heat spreading in the cell because of the very high thermal conductivity of the wound current collectors in the casing have large impact on the measured wall temperature.

For example, Kim et al. [26] give the average cell temperature during a local heating simulation of a cylindrical cell (50 mm diameter and 90 mm height) in Fig. 9a. If that curve is the only information taken into account, the average temperature of the cell is widely hotter than wall temperature measured in the electric heater in this study. The simulation conditions are different from the tests performed here because of a heat exchange coefficient of 5 W m^{-1} K^{-1}, with an ambient temperature value of 35 °C. In the current study, the ambient temperature is 20 °C under natural convection, in a battery module configuration. The authors provide temperature distributions in the cell, which shows a wall temperature around 82 °C after 30 min, whereas the initial temperature was 55 °C. So the temperature increased by 27 °C after 30 min. In the current study, the wall temperature raises from 20 °C to 79 °C in 30 min, so the temperature increase is 59 °C, which is quite higher compared to Kim et al. [26].

Santhanagopalan et al. [27] generate short circuits (S.C. in Fig. 9b) depending on their location in the Li-ion cell. They measured a higher wall temperature of a prismatic $LiCoO_2$/C cell when short circuit occurs between the negative current collector and the lithiated carbon electrode. The second higher peak is provided between the same materials, but with delithiated carbon. The third peak is about 100 °C, and appears when both current collectors are connected together. The order of magnitude of the maximum value and the shape of the curve can be compared to the Leising et al. [25] results (Fig. 9a), but the temperature rises faster (maximum temperature reached after 40 s). Then, Santhanagopalan et al. [27] provide two curves, which show a smaller thermal effect, when the short circuit is produced between the active material of both electrodes, or between the positive current collector and the positive electrode. The defect artificially generated in the current study presents the same order of magnitude that the smallest thermal runaway induced by Santhanagopalan et al. [27]. Finally, the tests called “thermal failure tests”, in that study, should be considered in quantitative terms, but the order of magnitude of the locally reached temperature for the entire module is sufficient to estimate qualitative results between the both thermal management systems.

Fig. 10a shows the wall temperature of the defective cell during thermal failure test for different cooling conditions. The natural convection cooling is the worst case among the three because of the quick temperature increase, up to 95.8 °C at the end of discharge (when SOC = 7%). The temperature of the cell passes over the battery manufacturer safety limit in 515 s. When forced convection

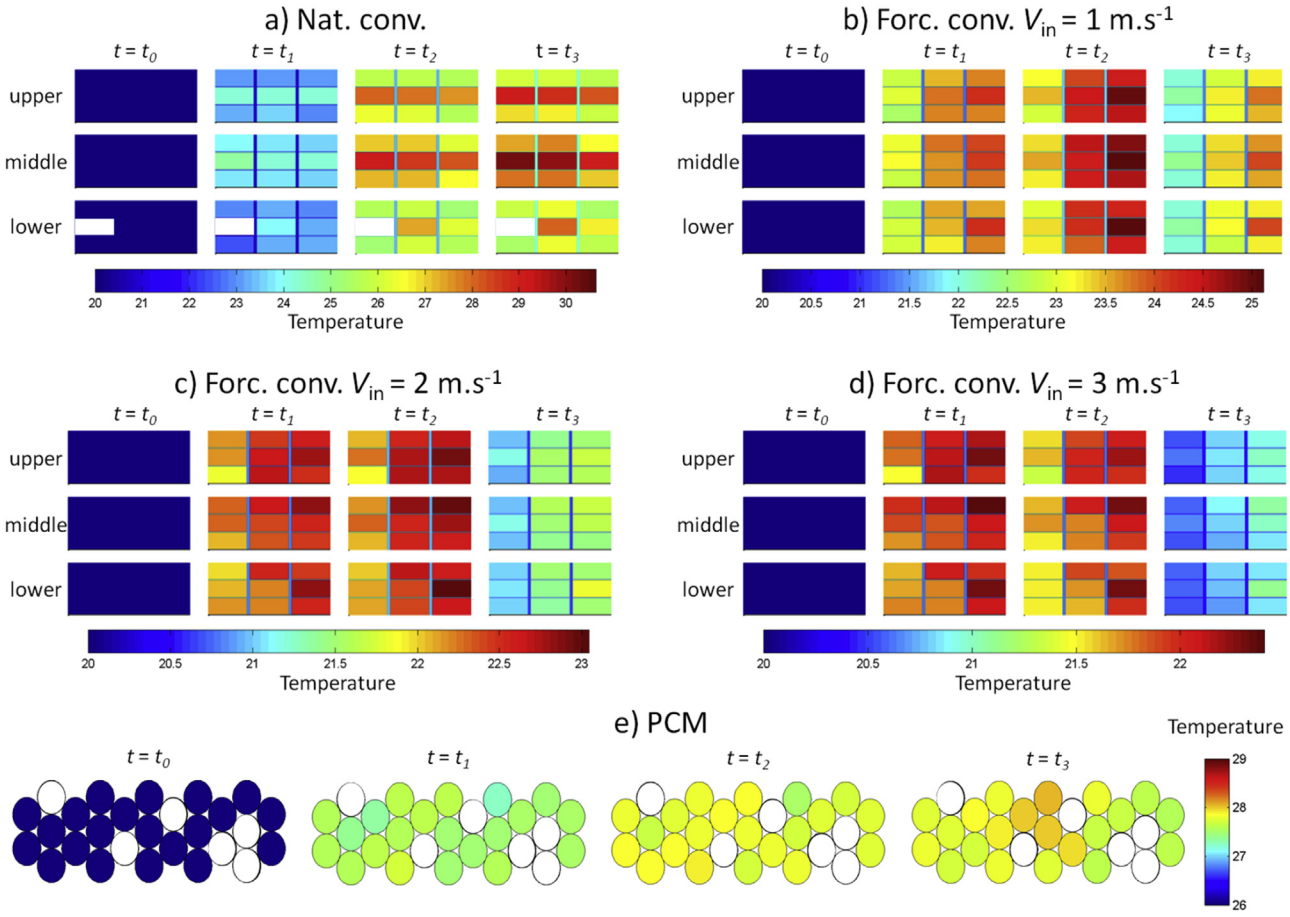

Fig. 8. Battery module temperature field vs. time depending on the battery thermal management system $t_0 = 0$ s, $t_1 = 1560$ s, $t_2 = 3125$ s, $t_3 = 4685$ s.

is used, with a 1 m s^{-1} inlet velocity, the temperature raise is a little slower, because of an improved heat exchange due to the flow. So the safety limit is exceeded in 902 s. Then the temperature rise is stopped because a thermal equilibrium is reached. The final temperature at the end of the discharge driving cycles is about 65.4 °C, which is over the manufacturers safety limit, and accelerates the aging of the cell. Because of the low thermal conductivity of the perpendicular direction to the electrodes, a quite higher

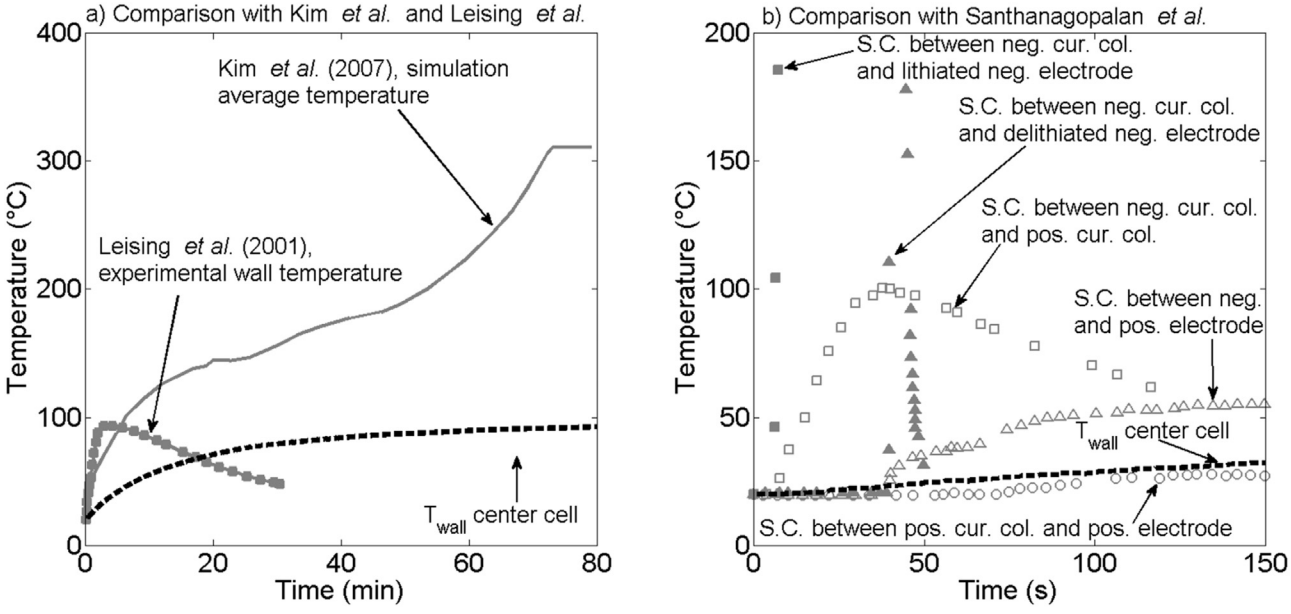

Fig. 9. Comparison between the wall temperature of the center cell and the literature data.

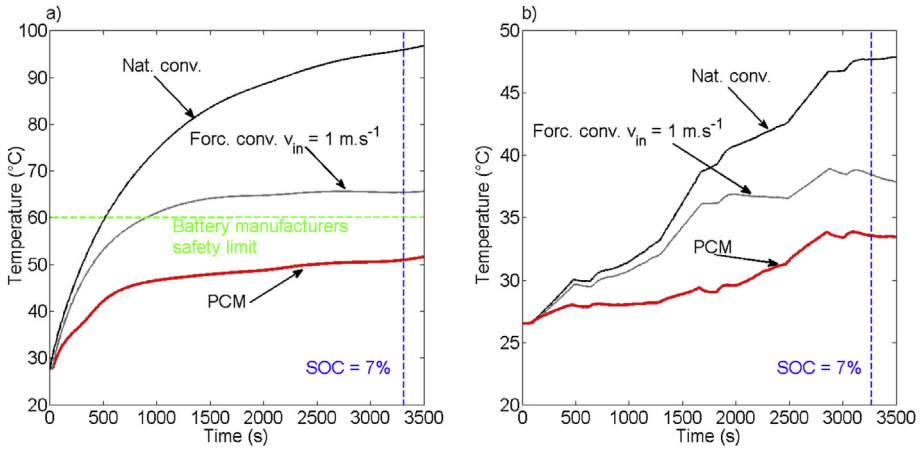

Fig. 10. a) Wall temperature of the defective cell and b) maximum wall temperature of the other cells in the module.

temperature inside the cell can be assumed. PCM battery management system shows good safety performance in that thermal failure test. The wall temperature of the defective cell never exceeds 60 °C, because the heat power is well extracted from the PCM. Moreover, in that test, the liquid cooling system is not working. So safety could be greatly improved if the liquid cooling system was activated. The maximum wall temperature reached with the PCM over 3500 s is about 51.6 °C.

Fig. 10b shows the hotter cell in the module which is not the defective one. Natural convection, as expected, generates the largest impact of defective cell over its neighbors. In that case, the temperature increase is about 21.2 °C, so it is 2.5 times higher than the increase of the average temperature under usual conditions. Under natural convection, the hotter cells in the module are the 6 cells near the defective one with same order of magnitude. As it was seen with usual conditions, forced convection induces a thermal imbalance in the battery module with cold upstream cells and hot downstream ones. Thermal failure test induces this behavior again with a significant thermal impact on the direct downstream cell. Its wall temperature is increased by 3.5 times compared to the average temperature under usual condition, with a 11.9 °C rise from the beginning of the thermal failure. Because of the defect, thermal failure with the PCM battery management system shows a thermal imbalance from the center to the external cells of the module. But the wall temperature increase of the most impacted cell is widely slower than in the both cases of convection. Because of the aluminum cans, the heat is extracted vertically from the inside to the outside of the module before it influences the other cells. So the temperature increase of the hotter cell is only 7.1 °C.

So, with a faster and more intensive thermal failure, it is expected that the PCM battery management system associated to the active liquid cooling system would be widely more efficient than other cooling systems and ensures greater safety conditions.

3.2. Fan power requirement

The forced convection air cooling requires power in order to generate the flow [17]. It can be estimated by the pressure losses and the flow rate for different fan efficiency values (because of a lack of data). The fan power requirement can be estimated for one module. The calculation for a battery pack size has been tried with a strong assumption. With that kind of cell, two thousand cells are needed to power a car (14 kWh energy battery pack), so it represents 74 similar modules to the one simulate here. Linear pressure losses can be assumed as a first approach in order to estimate power requirement for the entire battery pack. Then the proportion of consumed energy for 3 French EVs has been estimated according to a variable efficiency values. Finally, Fig. 11 reports the estimation of the part of the energy dedicated to the fan.

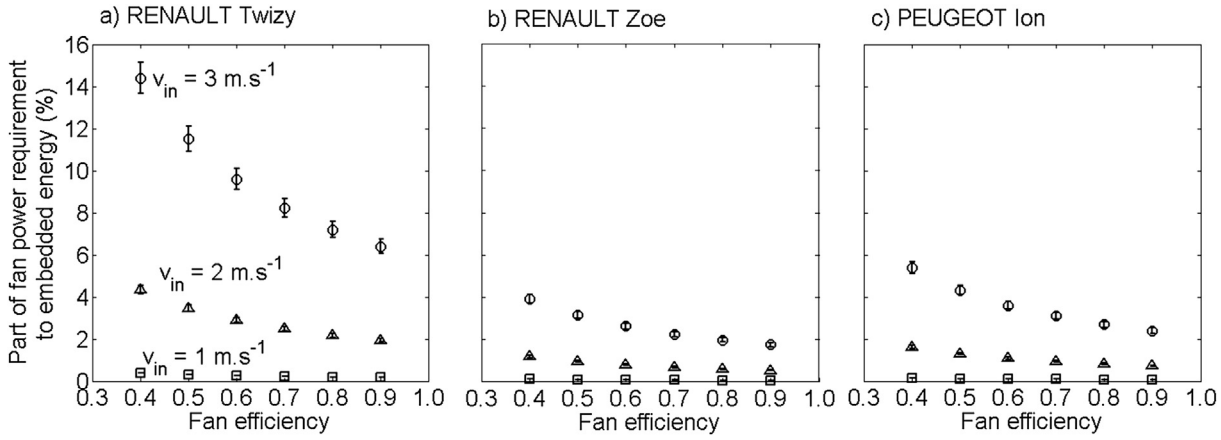

Fig. 11. Part of fan power requirement related to embedded energy for three French EVs.

The energy embedded in the 3 French cars is different. Renault Twizy is small electric vehicle with 6 kW h energy on-board compared to 22 kW h for a Renault Zoe. Peugeot ion is equipped with a 16 kW h battery pack. For the three vehicles a low cooling velocity has no impact on embedded energy, and the efficiency of the fan does not show a large influence during a discharge driving cycle. But when the air velocity is increased the part of energy used by the fan is more important and the efficiency becomes really important. The part of consumed energy depends widely on the size of the battery pack. An active cooling system is totally inappropriate for a small vehicle as Renault Twizy for example. In order to keep a quite uniform temperature field, a high inlet velocity is needed, but with an inefficient fan, more than 14% of the energy could be used to cool the battery. For bigger vehicles as Renault Zoe and Peugeot Ion, the part of the energy needed to cool the battery varies between 2 and 6%. At first, it seems to be quite small, but with the reduced part of the available energy in winter, it can become significant. To generate an inlet velocity of 3 m s^{-1} with a 0.4 efficiency fan, the battery should supply a power of 1 kW. Furthermore, air temperature needs to be controlled in order to keep the battery pack at a reasonable level of performance during summer or winter.

A computational fluid dynamics (CFD) simulation of 74 lined up modules has been performed for a 0.5C rate with a 1 m s^{-1} velocity and 20 °C temperature for the air at the inlet. A 34.9 °C wall temperature was estimated on the last cell at the end of the battery pack. So the temperature increases by 15 °C, from the upstream to the downstream of the battery pack, and the battery management system criteria are not validated.

Finally, an active air cooling system cannot be effective in terms of battery thermal management system because of energy consumption on one hand, and its disability to respect battery thermal management system criteria on the other hand.

3.3. Active PCM solidification

Although the PCM is a very interesting solution in order to keep all the cells in the battery module at the same temperature during discharge, heat needs to be evacuated after melting. Some authors enhanced the thermal conductivity of the PCM with a graphite matrix, which is light weight. But even if that thermal property is widely enhanced, the heat is not removed as quickly as in order to make a quick charge with a 2C rate after a discharge driving cycle.

That is why the battery management system presented here is equipped with two cooling plates in mechanical contact with aluminum cans with fins. The cans allow the use of a small PCM quantity (sufficient in order to keep a cell between 28 and 30 °C during a 3C rate discharge), which can be solidified quickly after melting when the liquid cooling system is working. A solidification test was performed. It consists of a discharge three driving cycles, followed with a 2C rate charge. The PCM solidification is performed during charge with the liquid cooling. The water temperature is regulated at 22 °C.

Fig. 12 shows the PCM solidification during a fast charge after a repetition of three driving cycles. At the end of the fast charge, every temperature probe provides a temperature lower than 26 °C, so the PCM is fully solidified. In that case, the power of temperature control is estimated at 300 W. The water temperature was regulated in the by-pass of the test section, whereas in reality the regulation of water temperature needs time and power before solidification of the PCM. That is why a second test was performed. It consists of 1C rate half charge, with water initially at 34 °C, regulated to 26 °C after the beginning of the charge. The charge succeeds two driving cycles. At the end of the half hour test, the PCM is not solidified in all the cans. A third of the cells have a wall temperature inferior or equal to 27 °C, but not the entire module. It is expected that a 25 °C water temperature of regulation to be sufficient in order to solidify the entire PCM. In that case, a heat power of around 400 W, including water temperature control, is transferred to the water. So it is expected that with a power lower than 1 kW, the entire PCM can be solidified during a 2C fast charge. So that system could be coupled to air conditioning system. The driver is generally out of the car during it is charging, so there is no need of air conditioned in the passenger compartment.

4. Conclusions

Two experimental setups were tested in order to compare natural and forced air cooling to a semi-passive PCM battery management system.

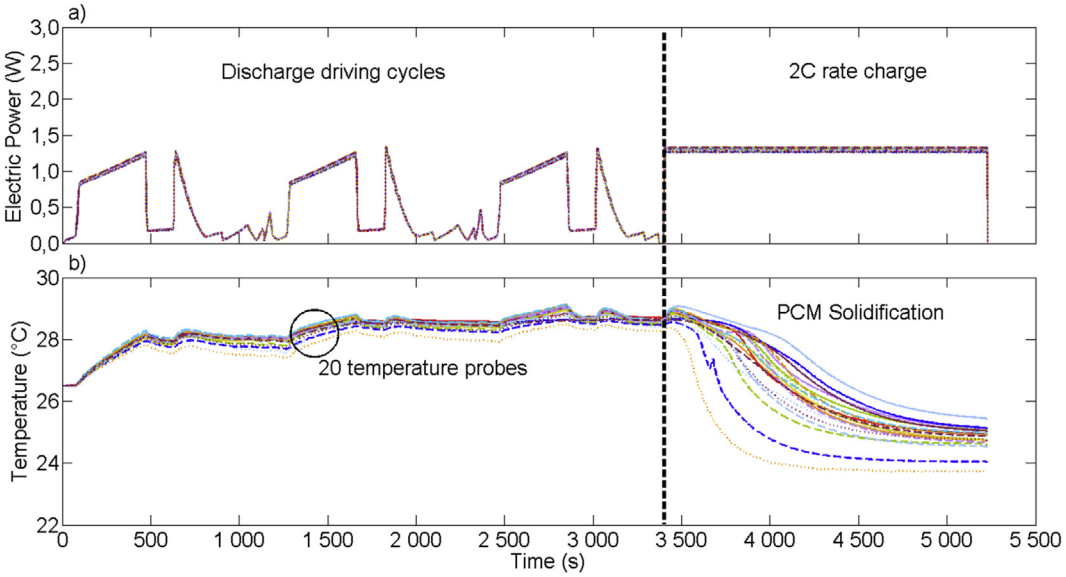

Fig. 12. PCM solidification during fast charge, a) electric power of cycle, b) temperature response.

Temperature distributions were presented for natural and different flow rates of forced convection. These two kinds of cooling induce temperature differences at a 27 cells battery module. The battery pack expansion suggests that battery thermal management criteria are not satisfied in terms of temperature discrepancies with a low inlet velocity. When the flow rate increases the fan power requirements become excessive if the fan has not a great efficiency. Under failure tests, the wall temperature of the defective cell exceeds the battery manufacturers safety limit of 60 °C with air cooling. The thermal defect spreads quickly to the surrounding cells.

The PCM battery management system improves widely the temperature uniformity during its melting, without any region significantly hotter than another. The wall temperature of the defective cell remains under 60 °C during the failure test. The average temperature of the other cells in the module is influenced by the defect, later and more weakly, than with natural or forced convection.

The PCM solidification when the battery experienced a 2C fast charge was a success. So the battery can undergo successive electric requests, as a charge following a discharge. A good behavior of the battery module is expected for cold cranking too.

The most important improvement, which can be lead on the PCM battery management system is weight reduction of the cans. The PCM-can/cell weight ratio is about 46.7%, compared to 28.6% obtained by Khateeb et al. [19], but the volume ratio is widely better, 25.0% in that study against 79.7%.The global weight ratio should take into account the liquid cooling system, but it is the order of magnitude of a liquid cooling battery management system alone. So with a can mass reduction, it is expected that the weight of the entire PCM battery thermal management system should not be much larger than that of a purely liquid system. The PCM/cell weight ratio is only 13.4% with that system.

Acknowledgment

The authors are grateful for the technical support provided by Mr. Paul Bonnamy, Mathieu Giraud, and the technicians of the CEA LETh.

References

[1] D. Bernardi, E. Pawlikowski, J. Newman, J. Electrochem. Soc. 132 (1985) 5–12.
[2] S. Paul, C. Diegelmann, H. Kabza, W. Tillmetz, J. Power Sources 239 (2013) 642–650.
[3] M. Fleckenstein, O. Bohlen, M.A. Roscher, B. Bäker, J. Power Sources 196 (2011) 4769–4778.
[4] J. Rugh, A. Pesaran, K. Smith, in: SAE Alternative Refrigerant and System Efficiency Symposium, 2011.
[5] Z. Rao, S. Wang, Renew. Sustain. Energy Rev. 15 (2011) 4554–4571.
[6] M.R. Cosley, M.P. Garcia, in: Telecommunications Energy Conference, Intelec 2004, 26th Annual International, 2004.
[7] J.-F. Cousseau, C. Siret, P. Biensan, M. Broussely, J. Power Sources 162 (2006) 790–796.
[8] C. Forgez, D.V. Do, G. Friedrich, M. Morcrette, C. Delacourt, J. Power Sources 195 (2010) 2961–2968.
[9] P. Nelson, D. Dees, K. Amine, G. Henriksen, J. Power Sources 110 (2002) 349–356.
[10] DOE/ID-10597, PNGV Battery Test Manual, Revision 3, February 2001.
[11] R. Mahamud, C. Park, J. Power Sources 196 (2011) 5685–5696.
[12] Q. Wang, P. Ping, X. Zhao, G. Chu, J. Sun, C. Chen, J. Power Sources 208 (2012) 210–224.
[13] P. Ramadass, B. Haran, R. White, B.N. Popov, J. Power Sources 112 (2002) 614–620.
[14] M. Sievers, U. Sievers, S.S. Mao, Forsch. Ingenieurw. 74 (2010) 215–231.
[15] R. Kizilel, A. Lateef, R. Sabbah, M.M. Farid, J.R. Selman, S. Al-Hallaj, J. Power Sources 183 (2008) 370–375.
[16] R. Kizilel, R. Sabbah, J.R. Selman, S. Al-Hallaj, J. Power Sources 194 (2009) 1105–1112.
[17] R. Sabbah, R. Kizilel, J.R. Selman, S. Al-Hallaj, J. Power Sources 182 (2008) 630–638.
[18] S. Al-Hallaj, R. Kizilel, A. Lateef, R. Sabbah, M.M. Farid, J.R. Selman, in: Vehicle Power and Propulsion, IEEE Conference, 2005.
[19] S.A. Khateeb, M.M. Farid, J.R. Selman, S. Al-Hallaj, J. Power Sources 128 (2004) 292–307.
[20] R.D. Metha, P. Bradshaw, Aeronaut. J. R. Aeronaut. Soc. (1979) 443–449.
[21] A. Sharma, V.V. Tyagi, C.R. Chen, D. Buddhi, Renew. Sustain. Energy Rev. 13 (2009) 318–345.
[22] Y. Inui, Y. Kobayashi, Y. Watanabe, Y. Watase, Y. Kitamaura, Energy Convers. Manag. 48 (2007) 2103–2109.
[23] K. Onda, H. Kameyama, T. Hanamoto, K. Ito, J. Electrochem. Soc. 150 (2003) A285–A291.
[24] G.-H. Kim, A. Pesaran, World Electr. Assoc. J. 1 (2007) 126–133.
[25] R.A. Leising, M.J. Palazzo, E.S. Takeuchi, K.J. Takeuchi, J. Electrochem. Soc. 148 (2001) A838–A844.
[26] G.-H. Kim, A. Pesaran, R. Spotnitz, J. Power Sources 170 (2007) 476–489.
[27] S. Santhanagopalan, P. Ramadass, J. Zhang, J. Power Sources 194 (2009) 550–557.